Mechanically Induced *g*-Jitter from Space Station Rotary Joints

Robert L. Boucher[(1)]

1. The Boeing Company, Mail Stop H020-F603, 5301 Bolsa Avenue, Huntington Beach California, USA 92649, (714) 899-8566, Robert.L.Boucher@boeing.com

Introduction

The mission of the International Space Station is to provide a working laboratory in orbit for research in engineering, life sciences, and microgravity. Among the microgravity disciplines that are preparing to utilize this international resource are materials processing, combustion, fluid dynamics, biotechnology, and fundamental physics[1]. The Station promises to enable significant advances in each of these areas by making available a research facility in which gravitational and other accelerations, and their corresponding buoyancy and diffusion effects on various physical processes, are orders of magnitude lower than they are on Earth.

In order to fulfill this promise, it is not enough for the Space Station to simply replicate a typical terrestrial scientific laboratory in orbit. Although an orbiting laboratory is free of most of the effects of gravitational acceleration by virtue of its free fall condition, it also produces structural vibration or jitter that can interfere with the processes under study. To ensure the quality of the acceleration environment and enable a successful mission, the Space Station Program has limited potential disturbances in two ways: first, by isolating the most sensitive payloads from the vehicle structure, and second, by quieting major disturbances at their sources. The first area, payload isolation, is implemented inside the pressurized modules at the rack level[2]. Sub-rack level isolators have also been developed.[3, 4, 5] This paper addresses the second area, disturbance source limits, for one of the major sources of mechanical noise on the Space Station: the Solar Alpha Rotary Joints.

Due to the potential for large disturbances to the microgravity environment, an initial analytical prediction of rotary joint vibration output was made[6]. Key components were identified and tested to validate the analytical predictions. Based on the component test results, the final vibration output of the joints was verified by a test on each fully assembled flight unit. This paper describes the Space Station microgravity requirements, the rotary joint hardware, and the disturbance producing aspects of joint operation. The test setup, instrumentation, test conditions, and results for the component level and system level measurements are described. An overall forcing function that describes the maximum torque imparted to the Station is created based on the test results, and these disturbances are shown to meet the applicable Space Station microgravity requirements.

Microgravity Requirements

Microgravity disturbance limits for the Solar Alpha Rotary Joint are separated into two general categories. Quasi-steady requirements limit very low frequency disturbances — specifically, disturbances at frequencies below 0.01 Hz. Vibratory requirements limit higher frequency disturbances in the range of 0.01 to 300 Hz. Disturbances in the vibratory category include

bearing noise, imbalance in pumps or fans, and torque ripple in drive motors. For both quasi-steady and vibratory disturbances, the overall Station requirements are given in terms of net acceleration limits at the payload racks. This is the form most useful to payload designers.

For the mechanically induced disturbances produced by the thermal radiator joints, the requirement of interest is the low frequency vibratory acceleration limit. Accelerations at the internal payload racks are limited to less than 1.6×10^{-6} *g* over the low frequency range of 0.01 to 0.1 Hz, increasing by 20 dB per decade in frequency up to 1.6×10^{-3} *g* at 100 Hz from all disturbance sources on the vehicle. The acceleration environment is capped at this level for frequencies from 100 to 300 Hz. These requirements were originally derived from an analysis of a single sinusoidal disturbance and its potential impact on various physical processes[7].

Each major hardware segment is sub-allocated a portion of the overall acceleration limit. The Solar Alpha Rotary Joints are located on the S3 and P3 truss segments, which have an allocation of 0.3×10^{-6} *g* at 0.01 Hz. The S3 and P3 allocation increases with frequency in the same way as the overall system specification.

Description Of Hardware

A view of the Space Station s assembly complete configuration is shown in Figure 1. Cylindrical pressurized modules enclosing the living and working space for the crew are visible in the center. The long lateral truss structure holds solar arrays, seen in pairs at each end; these large appendages must be rotated to track the sun. The Solar Alpha Rotary Joints (SARJ) are located along the main truss, just inboard of the solar arrays, and provide rotation about the truss axis to the outboard structure on either side.

The joint and its major components, including drive motor and structural bearings, are shown in Figure 2 through Figure 4 respectively. The motor includes a gearbox with two meshes in the drive train. The main structural bearings consist of twelve sets of three rollers each, evenly distributed about a race ring approximately 130 in diameter. The SARJ is capable of rotating continuously while passing 14 kW of electrical power across the joint. The large mass and inertia of the solar arrays and power system thermal radiators moved by the joint, over 52,000 lb and 5.8×10^9 lb-in^2 respectively, make it one of the largest potential microgravity disturbances on the Station.

Due to the presence of a second rotating bearing at the base of each solar array, the SARJ does not need to accommodate all of the variation in sun angles and orbital positions. The SARJ rotation only reflects the orbit rate, and thus turns at a relatively constant four degrees per minute. At assembly complete, the rotation rate is expected to vary less than 10% from this nominal value.

Rotary Joint Microgravity Disturbances

An ideal SARJ would turn perfectly smoothly, and therefore would not perturb the Lab s acceleration environment at all when operated at constant speed. In reality, however, several

electrical and mechanical effects interfere with smooth turning and thus produce microgravity disturbances.

The first group of disturbances are collectively called torque ripple. Contributors in this category include power amplifier internal offset, motor controller drive channel unbalance, motor winding unbalance, motor torque constant variation, and cogging torque. Power amplifier offset is actually a collection of several small offset errors from imperfect electrical components in the motor control circuit, including the current sensor, the summation circuit that compares commanded current to sensed current, and the signal amplifier. The net offset error is commutated with each electrical cycle, producing a small variation in the motor command signal and hence in the output torque. Drive channel unbalance arises from not-quite-identical gain in the power amplifier channels for the sine and cosine windings of the SARJ s two-phase DC motor. In addition, a perfect set of sine/cosine signals entering the motor will still produce torque ripple if the motor windings themselves are slightly unbalanced. The motor windings are required to be balanced to within 1% of the zero-to-peak drive current, which will appear as a disturbance at the second harmonic frequency. Torque constant variation is another similar effect; small non-uniformities in the placement of stator windings produce corresponding non-uniformities in the output torque of the motor. This results in disturbances at the second and higher harmonic frequencies. Finally, cogging torque is produced by the interaction of the rotor and stator magnetic fields, which results in a tendency for the rotor to favor certain discrete positions. This effect contributes disturbances at the first, second, fourth, and eighth harmonic frequencies as well as a small 1/12th harmonic component.

The second type of disturbance is caused by the position resolver. The SARJ controller feeds back both joint angle and rate, and the resolver that measures these quantities has precision limitations. Thus, there is a small error in the signal, which in turn generates a small irregularity in the SARJ s turning. To minimize this disturbance, the joint design includes a high precision resolver.

A third type of disturbance arises from the joint s gear train. The input gear has 18 teeth and the input shaft rotates once for each 12 electrical cycles of the motor, giving a gear mesh frequency of 18/12 = 1.5 times the motor electrical speed for the first mesh. The intermediate and output gears have 201 and 20 teeth respectively which produces a second gear mesh frequency at 20*18/201/12 = 0.15 times the motor electrical speed. Higher harmonics of these frequencies are also expected.

Finally, rolling friction in the joint s bearings presents another independent source of disturbances. The SARJ has two significant bearing disturbances: the main structural bearings and the Power and Data Transfer Assembly bearings. The main bearings, which contain 12 sets of 3 rollers on a 128 inch diameter race ring, constrain the SARJ in the axial and radial directions while allowing the joint to rotate. The power transfer bearings are part of the mechanism that allows power to cross from the rotating (relative to the orbital frame of reference) to the stationary portions of the Station. The drag torque of these bearings varies slightly as the SARJ turns, which acts as a disturbance to the control system. In addition, roller and race ring surface roughness create random noise during operation. It should be noted that unlike the previous

three types of disturbances, which are termed narrow-band because they occur at sharply defined frequencies, bearing friction is a wide-band disturbance with broad spectral content.

The rotary joint controller is utilized for active vibration compensation as much as possible. The rotary joint model is shown in a simplified representation in Figure 5. The complete model has voltage, current, angular rate and angular position control loops. The voltage and current loops (not shown) are very high bandwidth servos, with phase crossover frequencies of about 51 kHz and 600 Hz, respectively. The two-loop model shown approximates the closed current loop including motor load effects on current with the k_{rl} gain and the fourth order power amp/motor filter depicted in the figure. The rate and position loops are shown in their entirety, including all gains and filtering. By upgrading to a higher precision resolver and adding a mid-frequency gain boost to the rotary joint rate feedback loop, net accelerations at the laboratory were reduced by more than order of magnitude at some frequencies. A significant cost saving was achieved by using active compensation compared to purely mechanical solutions to improve the joint's vibration performance.

Verification Testing

The disturbances generated by the mechanical and electrical systems of the joint are measured by means of a differential velocity signal. The joint s main drive motor is equipped with an internal resolver that is used to measure its position and velocity continuously, and this information is fed back through the controller to compensate for any detected deviations from the commanded position and velocity. If the joint is commanded to a constant velocity, any changes in the motor current will be solely a reflection of the joint s internal measurement of the disturbances present in the system at the motor. This current signal, called velocity error, was recorded during joint ground testing and used to calculate the actual quantity of interest — the disturbances present at the output shaft of the gear train — by analytically factoring in the controller disturbance compensation and the end-to-end gear ratio.

One advantage of velocity error measurement is that it requires virtually no dedicated instrumentation. The velocity error is calculated continuously by the motor as part of its normal operation and is available on the internal data bus of the motor controller. All that is required is to query the bus at a sufficiently high rate to capture the frequency range of interest. For all SARJ testing, data was recorded at 25 Hz, and therefor sinusoidal components are characterized with at least 8 points per cycle up to 25/8 or about 3 Hz. Additional data with fewer data points per cycle is available up to the Nyqist frequency of 12.5 Hz, although the calculated spectral amplitudes are less reliable in this range.

Velocity error data was measured on the qualification unit and each flight unit of the SARJ. Each flight unit has two complete drive strings for redundancy and both were tested. Data was taken at a joint rate of 4 degrees per minute, the nominal operating speed, and also at a higher rate to identify which of the measured disturbance frequencies are proportional to the joint rate. Data was recorded at each speed in both clockwise and counterclockwise directions, and for the first flight unit at ambient, maximum, and minimum flight predicted temperatures in a vacuum. Finally, some data was taken with the motor running but the pinion gear backed off from joint output shaft. This eliminated all joint motion, leaving only motor operation. Since mechanical

bearing noise is thus eliminated from the measurement, the torque ripple and gear train disturbances alone are isolated.

Typical results from the velocity error measurements are shown in Figure 6 and Figure 7. The raw time history data set, in units of degrees per second (motor electrical), was cropped to remove startup and shutdown transients and de-trended by subtracting a linear least-squares fit. Following Fourier transformation, motor torque ripple and gear meshing disturbances are clearly visible, with the expected frequencies marked with light vertical lines in the resulting spectrum shown in Figure 6. Peaks at each of these frequencies are calculated by integrating the power spectrum at frequencies with spectral amplitudes above the noise floor. The peak and noise values are multiplied by the controller transfer function, taking into account the difference between test and on-orbit inertia loads, and converted to torque in units of in-lb. The result is integrated over one-third octave bands to produce the net narrow-band and wide-band forcing functions shown in Figure 7.

Validation Of Analytical Model

As noted previously, the microgravity measurements taken from the SARJ required significant analysis to produce a prediction of net on-orbit disturbance torque. Because of the impracticality to rotating the joint on the ground with its full inertia load, a much smaller inertia was used in the test configuration and the data was corrected accordingly. In addition, the velocity error measurement is upstream of the controller disturbance rejection and so this effect was also added analytically.

To gain confidence in the rotary joint performance model that was used for these purposes, tests were conducted on the drive motor, motor controller, and gear train. For example, Table 1 shows that the SARJ Drive/Lock Assembly brushless DC motor parameters show good agreement between the rotary joint model value, the specification, and the actual value based upon test measurements.

For the motor controller, the model values were compared with qualification test results at both the board level and for the entire unit end-to-end. The broad band boost filter board, which was added to the circuit to improve microgravity performance, shows excellent agreement between the test specifications, actual qualification unit test data and model predictions with differences ranging from about 0.1 dB to 0.4 dB up to 200 Hz. The power amp filter board shows similar agreement with differences ranging from about 0.1 dB to 0.5 dB up to 90 Hz. The end-to-end test examined the RJMC frequency response over frequency, signal amplitude and temperature. Agreement is excellent between the actual RJMC qualification test data and model predictions up to 94 Hz with differences about 0.1 dB to 1 dB. Model usage in this case was for performance assessments below 12.5 Hz.

Results

Evaluation Of SARJ Motor Data

The SARJ test data was expected to contain spectral peaks at many frequencies. The motor torque ripple, intermediate gear mesh, and output gear mesh were all expected to contribute narrow band peaks at their fundamental frequency as well as higher harmonics of that frequency. Figure 6 shows an example of these peaks in the velocity error data. Note that while motor ripple and intermediate gear mesh frequencies are clearly evident, output gear mesh frequencies are not. This indicates that output mesh disturbances are not being transmitted through the gear train back to the motor where velocity error is sensed.

An unexpected peak is evident at 0.067 Hz. This is one half the motor electrical frequency and six times the motor mechanical frequency. The peak appears consistently in the data taken from various motor speeds, temperatures, drive units, and rotation directions, and its frequency is proportional to the motor speed. A second unexpected peak appears at one-third the motor electrical frequency, but not in all test cases. A comprehensive gear train signature analysis was performed to determine the frequencies characteristic of both normal operation and fault conditions[8]. This analysis calculates expected frequencies due to gear meshes and bearings, including both normal operation and fault indicators. The results, which are summarized in Table 2, do not show that the unexpected peaks correspond to any frequencies characteristic of the gears or bearings. The source of these peaks is still under investigation.

Trends In The Data

Tested conditions for the SARJ microgravity test included operation in both clockwise and counterclockwise directions, primary and redundant drive strings, engaged and disengaged pinion gear, and nominal and extreme values of joint rate and operating temperature.

Data was recorded for 900 seconds at 25 samples per second for each test condition, and a spectrum produced to look for characteristic frequencies as shown in the previous sections. In addition, several key frequencies were selected for a trend analysis showing their variation over the range of test conditions. These included the motor mechanical, motor electrical 1st and 2nd harmonics, and meshing frequencies of both gear sets. The trends in the peak disturbance values at these frequencies with changes in drive direction, drive unit, pinion gear engage state, joint rate, and operating temperature are discussed in this section.

Test results from the different drive strings of each SARJ were expected to be essentially the same, with the only differences due to manufacturing tolerances. Indeed the motor electrical 2nd harmonic results show this, as seen in Figure 8. In this figure, the results of individual test runs are plotted as points, with solid lines connecting runs that are identical in all respects except for drive unit. Some values go up slightly, some go down, but overall there is no consistent trend. Microgravity disturbances from the motor tended to be higher at colder temperatures as shown in Figure 9. None of the characteristic frequencies under review showed a consistent and significant trend with joint operating speed or rotation direction.

Torque Disturbance Estimate

The SARJ test data described in above was enveloped to create a single set of forcing functions for microgravity performance assessment. The discrete frequency and noise disturbances, respectively, are captured in the narrow band and wide band forcing functions shown in Figure 10. This data represents an envelope of all test conditions after analytically accounting for the effects of gear train dynamics and the increased inertia load during on-orbit operations. The gear train stiffness turned out to be a significant factor; the effects of a torsional resonance at 0.6 Hz are evident in the figure in the peak values at that frequency and the linear trends above and below it. Data above the Nyquist frequency of 12.5 Hz is an extrapolation.

The SARJ controller torque shown in Figure 10 is applied to the Station by a motor and gear train located on the perimeter of the joint. The gear applies a net torque to the radiator, with an equal and opposite torque reacting against the S3 or P3 truss segment. For assessment of SARJ performance against microgravity vibration output limits, this torque was multiplied by a structural transmissibility function that captures the propagation of SARJ disturbances through the truss to the location of sensitive payloads[9]. The results are shown in Figure 11. The results are less than the required limit in every frequency band, with a minimum margin of 1.2 in the 0.4 Hz band.

Conclusion

The quality of the Space Station microgravity environment is of great interest to researchers around the world. Ensuring that the mechanical equipment on Space Station does not unduly disturb this environment is of paramount importance in meeting the Station s research mission. Results of the rotary joint test program presented here show that the joints meet their allocation of the Space Station microgravity vibration limit, ensuring that this unique laboratory for microgravity research will not be adversely affected by the operation of one of the largest moving mechanisms on board.

Acknowledgements

The author is indebted to his supervisor at The Boeing Company, Mr. James Peebles, for his support and assistance. Mr. Daniel Nowlan, Boeing Technical Fellow, performed the control system analysis described in this paper. Mr. David Putnam of Lockheed Martin Corporation directed the joint testing. This work was performed under contract HX3200 from the National Aeronautics and Space Administration.

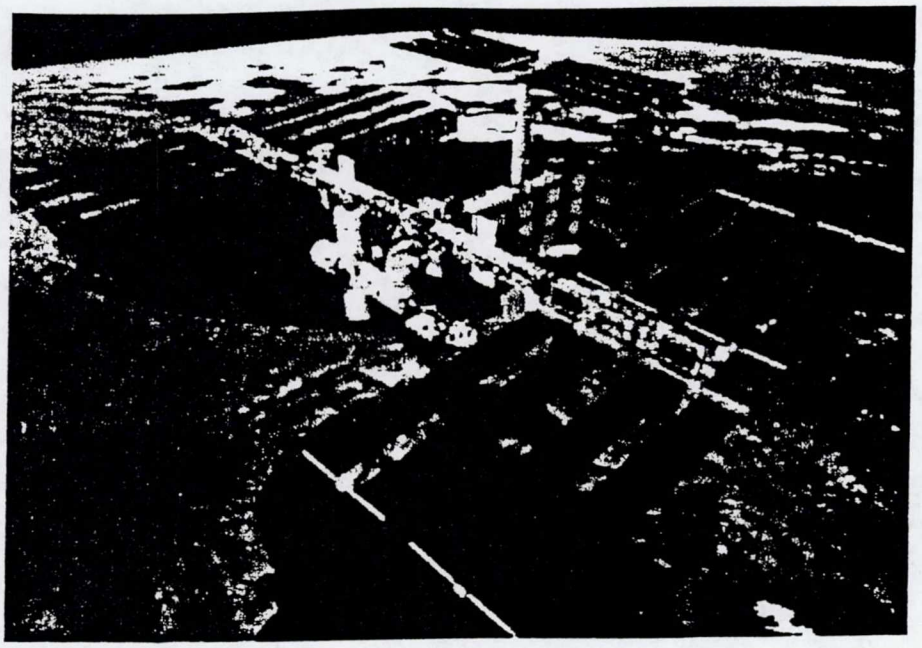

Figure 1. The Space Station's assembly complete configuration, with two sets of three thermal radiator panels flanking the central pressurized modules.

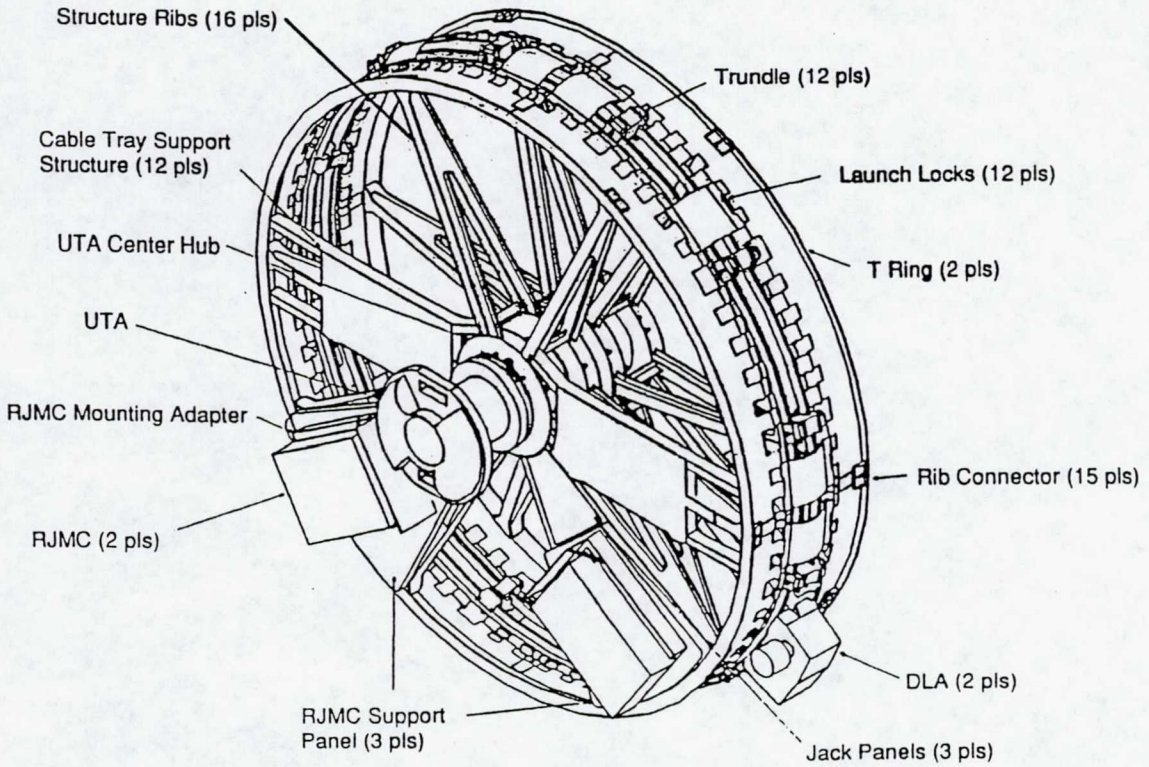

Figure 2: The Solar Alpha Rotary Joint.

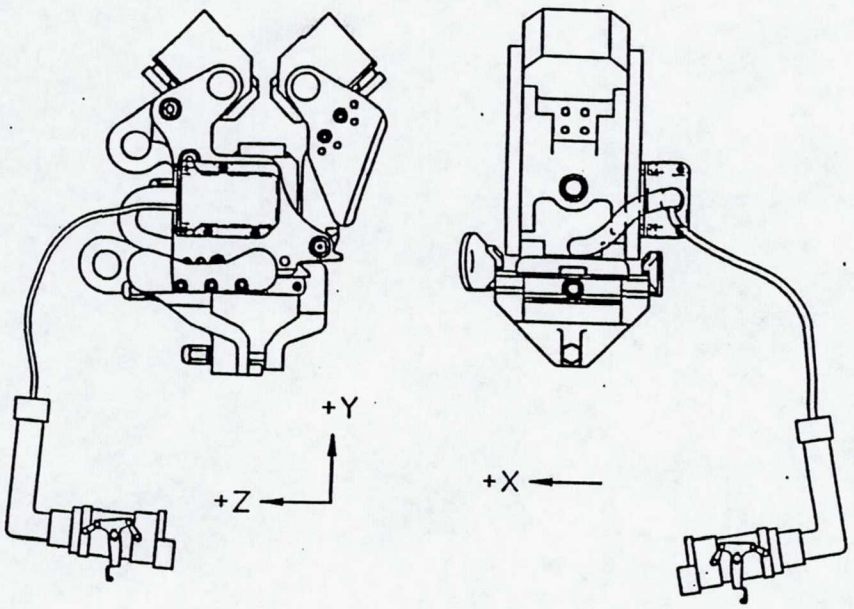

Figure 3. One of the twelve trundle bearings, each containing three rollers.

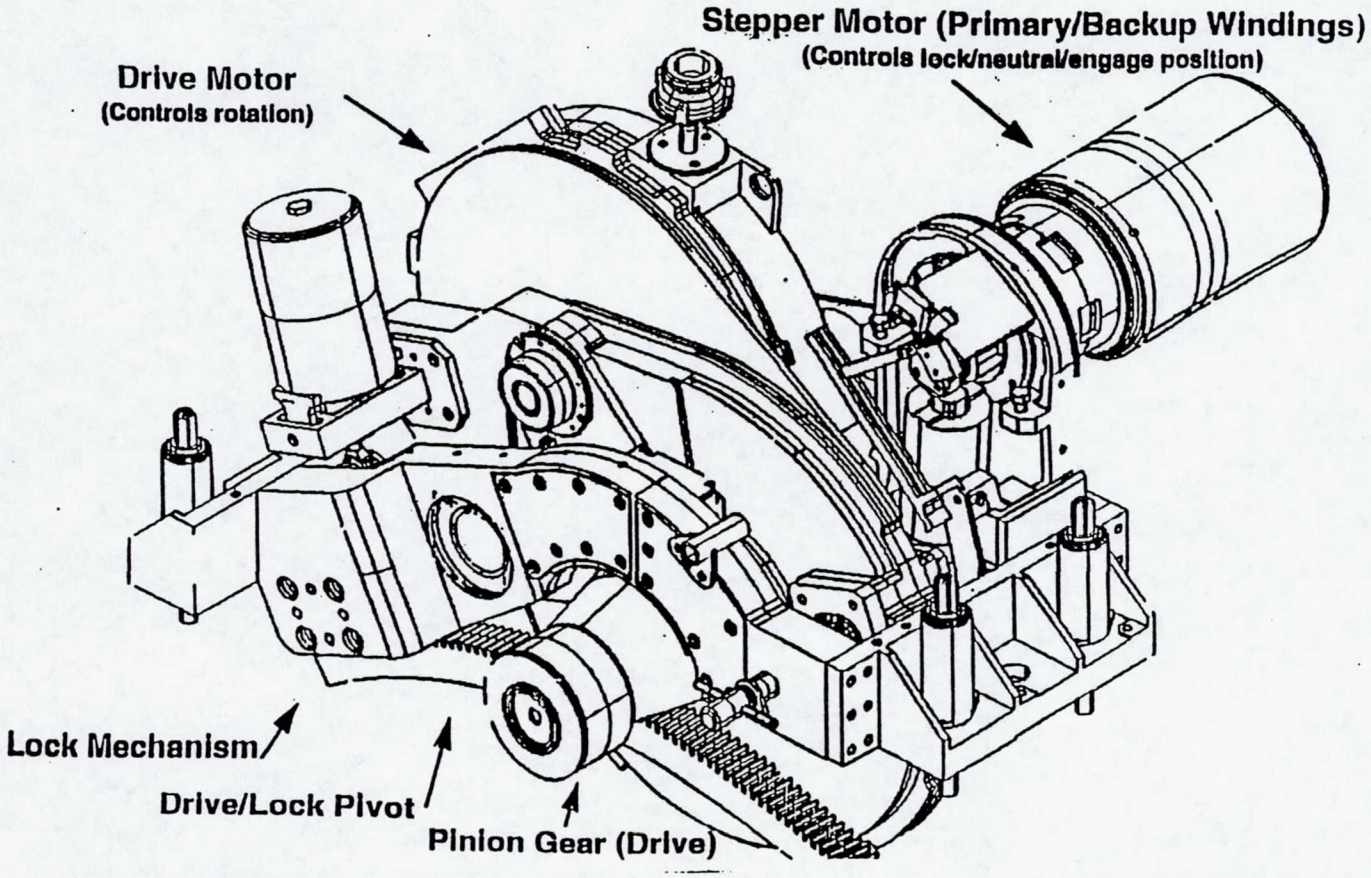

Figure 4. The Drive/Lock Assembly, which includes the primary torque motor for rotating the joint.

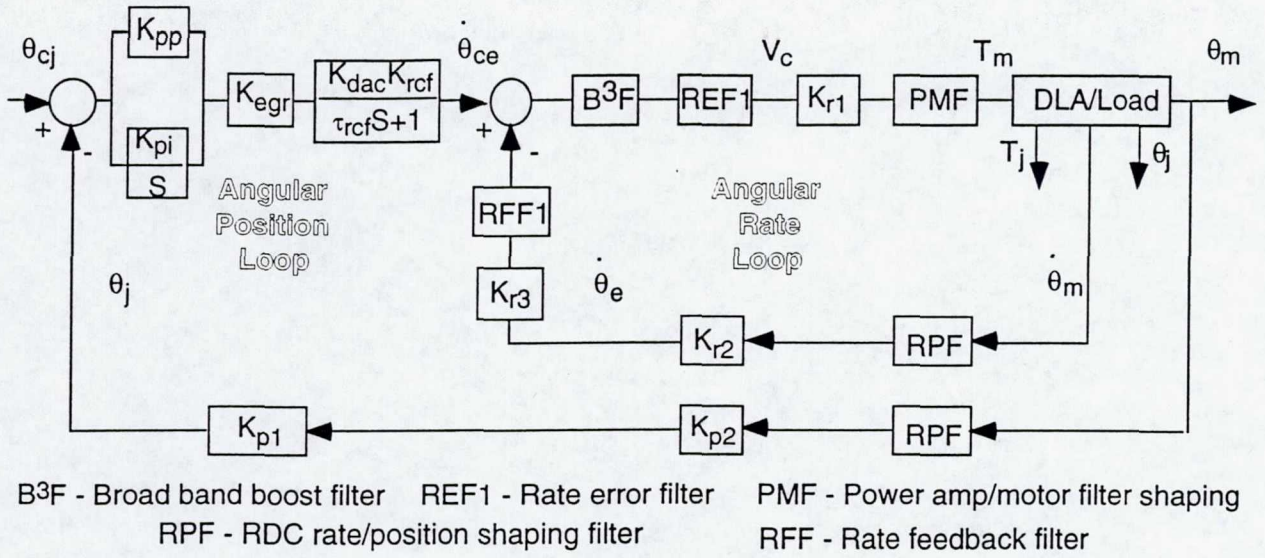

Figure 5. The low frequency response of the rotary joint control system is determined by the rate and position loops.

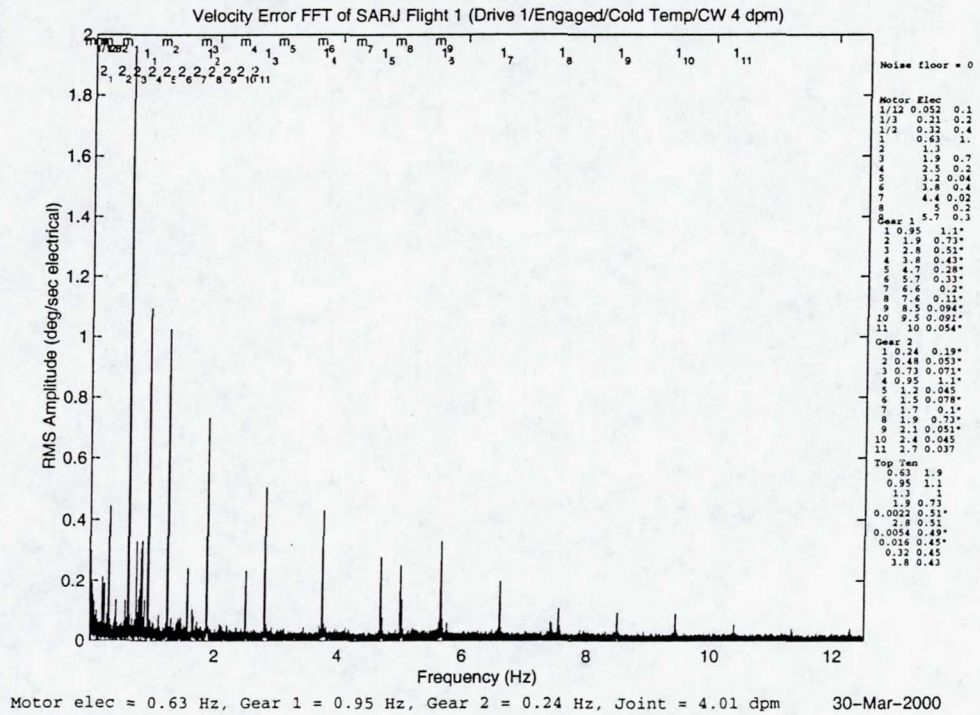

Figure 6. A velocity error spectrum shows peaks at the motor torque ripple and intermediate gear mesh frequencies (marked by m s and 1 s, respectively).

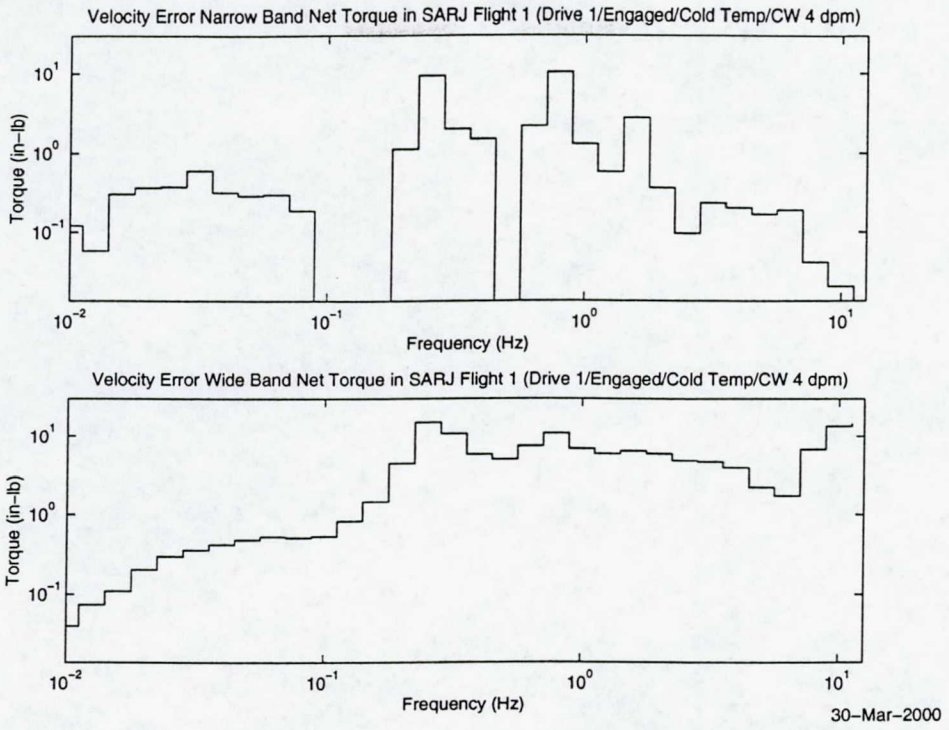

Figure 7. Accounting for the controller disturbance compensation and the different load inertias between the on-orbit and test configurations produces net joint torque in units of in-lb, which is then integrated in one-third octave bands.

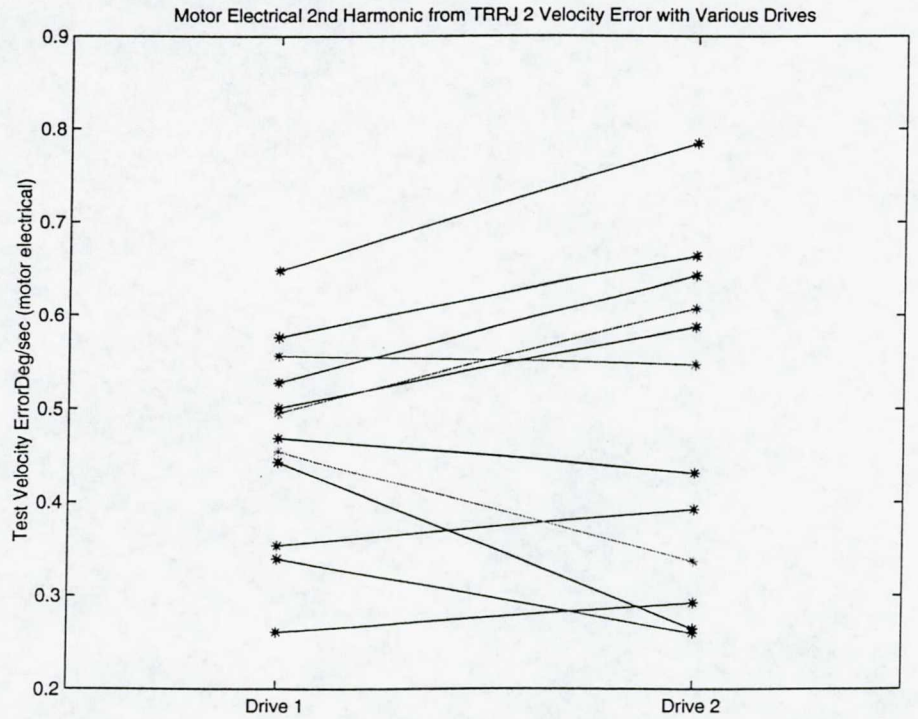

Figure 8. As expected, motor electrical 2nd harmonic results do not show a consistent trend with variation in the drive unit.

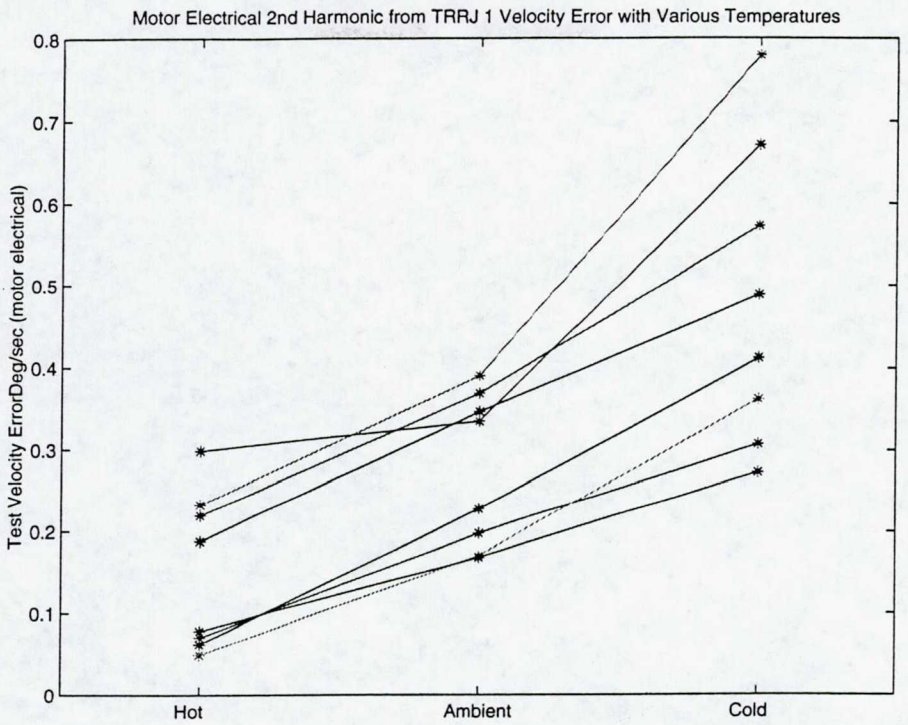

Figure 9. Motor related disturbances tended to increase at colder temperatures.

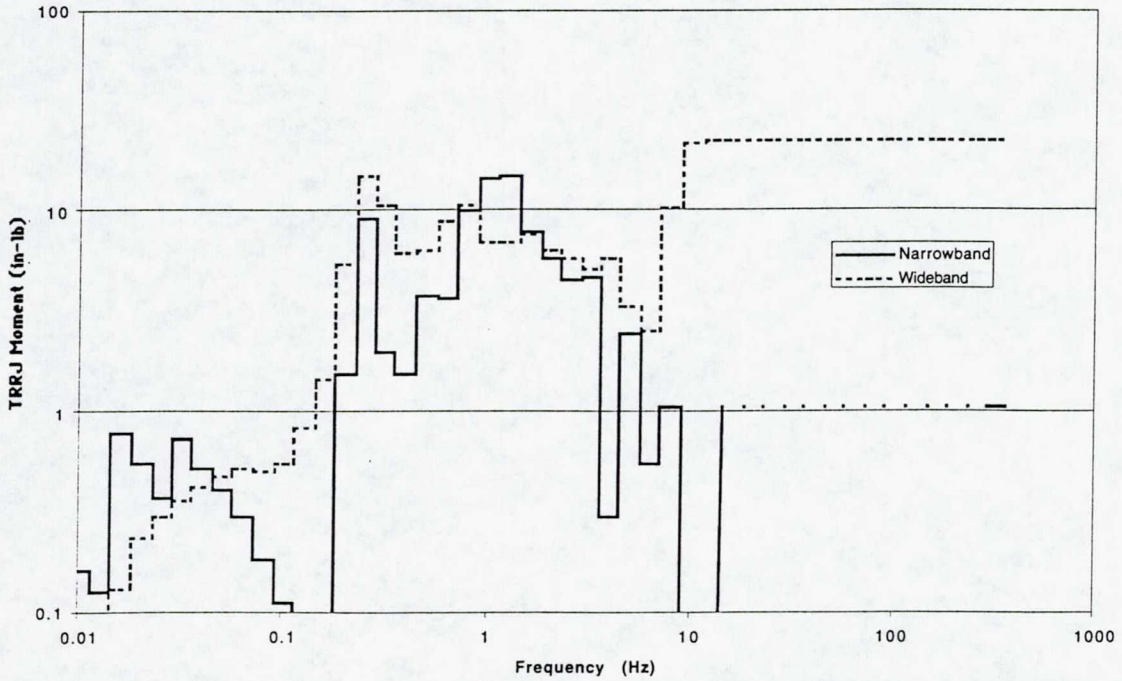

Figure 10. Wide-band and narrow-band disturbances enveloping all SARJ test conditions are used for microgravity assessment purposes.

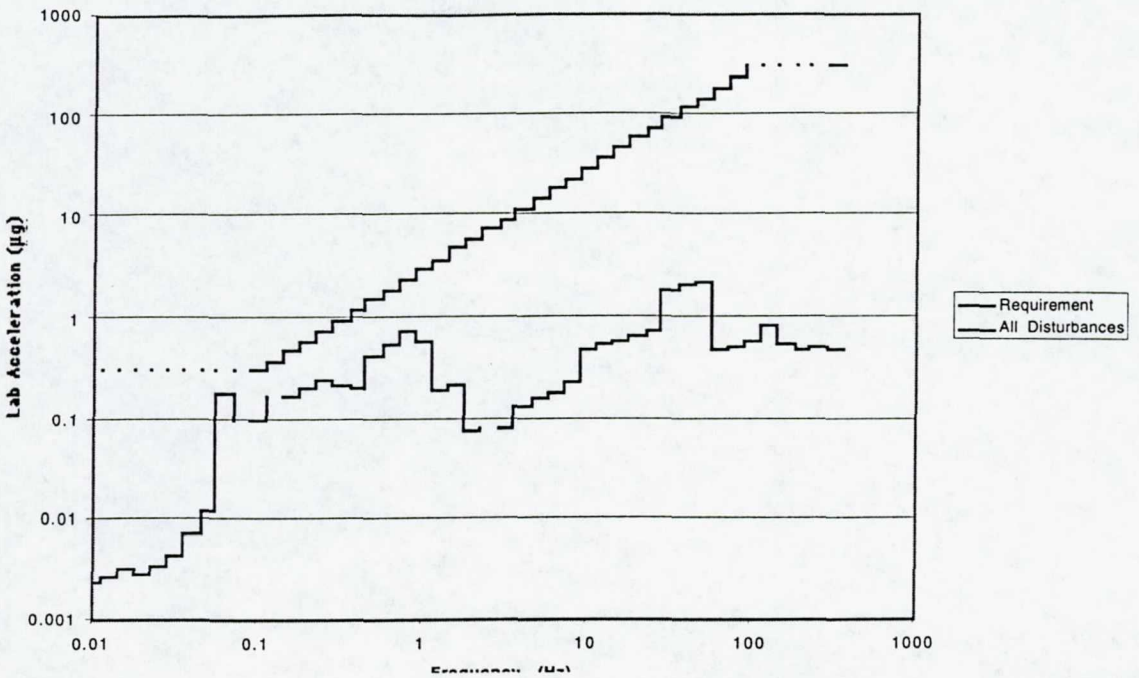

Figure 11. Test data shows that the rotary joint meets the Space Station vibration output limit.

Table 1. TDLA Brush-less DC Motor Parameter Comparisons

Unit	Avg. Winding Resist-ance (Ohms)	Average Induct-ance (mH)	Back EMF (volts/rad/sec)	Torque Constant (ft-lb/amp)
RJ Model	28.0	134	9.21	6.8
Spec Value	28 ± 2.24	134 ± 20%	9.21 ± 0.74	6.8 ± 8%
S/N 001	27.7	132	9.35	6.90*
S/N 002	27.7	127	9.38	6.92
S/N 003	28.0	130	9.31	6.87*
S/N 004	28.5	127	9.37	6.91
S/N 005	28.3	125	8.88	6.55*

*Calculated from back EMF (no test data available)

Table 2. Gear and bearing signature analysis for a joint rate of 4 deg/min.

Gear Set	Characteristic	Har-monic	Frequency
2	Hunting tooth		5.32E-06
2	Joint mechanical		5.32E-05
1	Hunting tooth		1.68E-04
2	Reducer shaft		1.01E-03
1	Reducer shaft		1.01E-03
	Bearing cage precession		5.52E-03
2	Assembly pass		1.01E-02
1	Motor mechanical		1.12E-02
2	Pinion eccentricity (-)		1.91E-02
2	Gear eccentricity (-)		2.01E-02
2	Mesh		2.01E-02
2	Gear eccentricity (+)		2.02E-02
2	Pinion eccentricity (+)		2.11E-02
2	Mesh harmonic	2	4.03E-02
2	Mesh harmonic	3	6.04E-02
1	Assembly pass		6.74E-02
2	Mesh harmonic	4	8.05E-02
2	Mesh harmonic	5	1.01E-01
2	Mesh harmonic	6	1.21E-01
	Motor electrical		1.35E-01
2	Mesh harmonic	7	1.41E-01
2	Mesh harmonic	8	1.61E-01
2	Mesh harmonic	9	1.81E-01
1	Pinion eccentricity (-)		1.91E-01
1	Gear eccentricity (-)		2.01E-01
2	Mesh harmonic	10	2.01E-01
1	Mesh		2.02E-01
1	Gear eccentricity (+)		2.03E-01
1	Pinion eccentricity (+)		2.13E-01
	Electrical harmonic	2	2.70E-01
	Ball spin		3.35E-01
1	Mesh harmonic	2	4.05E-01
	Electrical harmonic	3	4.05E-01
	Electrical harmonic	4	5.39E-01
1	Mesh harmonic	3	6.07E-01
	Ball fault (-)		6.65E-01
	Electrical harmonic	5	6.74E-01
	Ball fault (+)		6.76E-01
	Outer race fault		7.95E-01
1	Mesh harmonic	4	8.09E-01
	Electrical harmonic	6	8.09E-01
	Inner race fault (-)		8.11E-01
	Inner race fault (+)		8.34E-01
	Electrical harmonic	7	9.44E-01
1	Mesh harmonic	5	1.01E+00
	Electrical harmonic	8	1.08E+00
1	Mesh harmonic	6	1.21E+00
	Electrical harmonic	9	1.21E+00
	Electrical harmonic	10	1.35E+00
1	Mesh harmonic	7	1.42E+00
1	Mesh harmonic	8	1.62E+00
1	Mesh harmonic	9	1.82E+00

References

1 Karchmer, A., and Schafer, C., International Space Station Microgravity Research Requirements, AIAA 99-0571, 37th Aerospace Sciences Meeting and Exhibit, Reno NV, January 1999.

2 Active Rack Isolation System Development for the International Space Station, Bushnell, Anderson, Becraft, and Jacot, AIAA 97-1203, 38th SDM Conference, Kissimmee FL, April 1997.

3 Whorton, Mark, g-LIMIT: A Vibration Isolation System for the International Space Station, submitted to the Spacebound 2000 conference, Vacouver B.C. , Canada, 15-17 May 2000.

4 Tryggvason, Bjarni et. al., Acceleration levels and operation of the Microgravity Vibration Isolation Mount (MIM) on the Shuttle and the Mir space station, AIAA 99-0578, 37th Aerospace Sciences Meeting and Exhibit, Reno NV, January 1999.

5 Edberg, Donald, Nurre, Gerald, and Whorton, Mark, Performance assessment of the STABLE Microgravity Vibration Isolation Flight Demonstration, AIAA Paper 97-1202, 38th Structures, Structural Dynamics and Materials Conference, Kissimmee FL, April 1997.

6 Identification and Mitigation of Low Frequency Vibration Sources on Space Station, R. Boucher, AIAA 96-1205, AIAA Dynamics Specialists Conference, Salt Lake City UT, April 1996.

7 Nelsen, Emily S., An Examination of Anticipated g-Jitter on Space Station and its Effects on Materials Processes, NASA TM 103775, September 1994.

8 S&V Geometry 101, George Fox Lang, *Sound and Vibration,* May 1999, pages 16 — 26.

9 Crenwelge, O., Thampi, S., and Sun, W., ISS Vibratory Microgravity Environment: Disturbances, Transfer Functions, and Responses, AIAA 99-0572, 37th Aerospace Sciences Meeting and Exhibit, Reno NV, January 1999.